YAP enhances mitochondrial OXPHOS in tumor-infiltrating Treg through upregulating Lars2 on stiff matrix

Jingchao Bai [iD],[1,2,3] Meinan Yan,[1,2,3] Yihan Xu,[1,2,3] Youhui Wang,[1,2,3] Yuan Yao,[1,2,3] Peng Jin,[2,3,4] Yuhan Zhang [iD],[1,3] Yang Qu,[1,2,3] Liling Niu,[1,2,3] Hui Li[1,2,3]

[1]Department of Gastrointestinal Cancer Biology, Tianjin Medical University Cancer Institute & Hospital, Tianjin, China
[2]Tianjin Key Laboratory of Digestive Cancer, Tianjin's Clinical Research Center for Cancer, Tianjin, China
[3]National Clinical Research Center for Cancer, Tianjin Medical University Cancer Institute & Hospital, Tianjin, China
[4]Department of Gastric Surgery, Tianjin Medical University Cancer Institute and Hospital, Tianjin, China

Correspondence to
Professor Hui Li;
lihui05@tmu.edu.cn

ABSTRACT

Background Tumor-infiltrating regulatory T cells (TI-Tregs) are well-adapted to thrive in the challenging tumor microenvironment (TME) by undergoing metabolic reprogramming, notably shifting from glycolysis to mitochondrial oxidative phosphorylation (OXPHOS) for energy production. The extracellular matrix is an important component of the TME, contributing to the regulation of both tumor and immune cell metabolism patterns by activating mechanosensors such as YAP. Whether YAP plays a part in regulating TI-Treg mitochondrial function and the underlying mechanisms are yet to be elucidated.
Methods To gain insights into the effect of matrix stiffness on YAP activation in Tregs, alterations in stiffness were performed both *in vitro* and *in vivo*. YAP conditional knockout mice were used to determine the role of YAP in TI-Tregs. RNA-seq, quantitative PCR, flow cytometry, lentivirus infection and mitochondrial function assay were employed to uncover the mechanism of YAP modulating mitochondrial function in TI-Tregs. A YAP inhibitor and a low leucine diet were applied to tumor-bearing mice to seek the potential antitumor strategy.
Results In this study, we found that YAP, as a mechanotransducer, was activated by matrix stiffness in TI-Tregs. A deficiency in YAP significantly hindered the immunosuppressive capability of TI-Tregs by disrupting mitochondrial function. Mechanically, YAP enhanced mitochondrial OXPHOS by upregulating the transcription of *Lars2* (Leucyl-tRNA synthetase 2, mitochondrial), which was essential for mitochondrial protein translation in TI-Tregs. Since Lars2 relied much on its substrate amino acid, leucine, the combination of a low leucine diet and YAP inhibitor synergistically induced mitochondrial dysfunction in TI-Tregs, ultimately restraining tumor growth.
Conclusions This finding uncovered a new understanding of how YAP shapes mitochondrial function in TI-Tregs in response to mechanical signals within the TME, making the combined strategy of traditional medicine and diet adjustment a promising approach for tumor therapy.

WHAT IS ALREADY KNOWN ON THIS TOPIC

⇒ Tumor-infiltrating regulatory T cells (TI-Tregs) exhibit remarkable adaptability to the harsh tumor microenvironment (TME), they can switch to mitochondrial oxidative phosphorylation (OXPHOS) as their primary energy supply. Elucidating the underlying mechanisms of how TI-Tregs acquire metabolic fitness in the TME may yield clinical benefits.

WHAT THIS STUDY ADDS

⇒ We found that YAP, as a mechanotransducer, was activated by matrix stiffness in TI-Tregs, thus enhancing mitochondrial OXPHOS through upregulating Leucyl-tRNA synthetase 2, mitochondrial (Lars2), which was essential for mitochondrial protein translation. Since Lars2 relied much on its substrate amino acid, leucine, the combination of a low leucine diet and YAP inhibitor synergistically induced mitochondrial dysfunction in TI-Tregs, ultimately restraining tumor growth.

HOW THIS STUDY MIGHT AFFECT RESEARCH, PRACTICE OR POLICY

⇒ This study, for the first time, uncovered that YAP could enhance mitochondrial OXPHOS in TI-Tregs in response to mechanical signals within the TME. It highlights the potential of a combined strategy involving traditional medicine and dietary adjustments as a promising approach for tumor therapy.

BACKGROUND

Tumor-infiltrating Treg cells (TI-Tregs) play a pivotal role in facilitating the immunotolerance of malignant cells, ultimately contributing to unfavorable prognoses in numerous cancer types.[1] TI-Tregs exhibit remarkable adaptability to the harsh tumor microenvironment (TME), characterized by hypoxia, acidity, and nutrient deprivation, conditions that are often intolerable for other immune cells.[2] Previous studies suggest that TI-Treg possess a distinct metabolic profile from other T cells or Tregs in peripheral tissues,[3 4] they can uniquely use lactic acid and fatty acid as an energy fuel, and switch to mitochondrial oxidative phosphorylation (OXPHOS) as their primary energy supply.[5] Enhanced mitochondrial function, which governs metabolic reprogramming from glycolysis to oxidative metabolism, is crucial for Treg differentiation.[6] Elucidating the underlying mechanisms of how TI-Tregs

acquire metabolic fitness in the TME may yield clinical benefits.

The extracellular matrix (ECM) is an important molecular component of the TME, it not only provides a physical scaffold for cells but also contributes to the regulation of both tumor and immune cell metabolism patterns by activating mechanosensors.[7 8] Stiffness-mediated energy metabolism is crucial in regulating cell behavior and fate.[9–11] Notably, YAP, a well-known mechanotransducer, is responsive to various mechanical cues, particularly ECM stiffness,[12] and it subsequently orchestrates a broad spectrum of biological behaviors.[13] Evidence indicates that the role of ECM stiffness in immunity is complex and highly dependent on the specific immune cell type. YAP performs an immunosuppressive function in CD8+ T cells, particularly in the context of activated cytotoxic cells in the TME.[14] The stiffness of the matrix has the potential to stimulate the activation of YAP in CD4+ and CD8+ effector T cells, subsequently inhibiting metabolic reprogramming by impeding the nuclear translocation of NFAT1.[15] YAP activation caused by increased ECM stiffness impairs effector T cell proliferation, differentiation and cytotoxic function.[16 17] However, unlike in effector T cells, YAP is highly expressed in Treg and bolsters Foxp3 expression by upregulation of activin signaling,[18] whether there are other mechanisms behind it nor the reason for YAP activation in Treg is still not clear. Single-cell RNA-Seq reveals that induced Treg cells (iTregs) on stiffer substrates involve greater use of OXPHOS, and inhibition of ATP synthase reduces the rate of Treg induction,[19] indicating that matrix stiffness could influence mitochondrial function during Treg induction, but it is unclear whether YAP is involved in this process.

Here, our research reveals that a stiff matrix enhances TI-Tregs immunosuppressive capacity by potentiating mitochondrial OXPHOS. YAP provides a link between mechanotransduction and energy metabolism in TI-Tregs by increasing *Lars2* (Leucyl-tRNA synthetase 2, mitochondrial) transcription, which is crucial for mitochondrial protein translation relying on its substrate, the essential amino acid leucine. YAP inhibitor combined with low leucine uptake synergistically causes mitochondrial dysfunction in TI-Tregs, making the combination of traditional medicine with diet adjustment a promising strategy for cancer therapy.

MATERIALS AND METHODS
Mice
C57BL6/J *Foxp3*[cre] mice (here indicated as WT mice in our study) were purchased from the Jackson Laboratory (Strain #: 016959) , the *YAP*^{fl/fl} mice were purchased from Shanghai Model Organisms Center (Cat. No: NM-CKO-200174). The *YAP*^{fl/fl} mice were first crossed with *Foxp3*[cre] mice to generate F1 mice, then the F1 mice were inbred to generate the homozygous *Foxp3*[cre] *YAP*^{fl/fl} mice (here indicated as YAP-cKO mice in our study). Mice genotyping was performed using TaKaRa Taq V.2.0

plus dye (Takara, RR901A) according to the protocol with the following primers:

Foxp3-cre:
(Wild type Forward) CCCTTGACCTCAAAACCAAG,
(Mutant Forward): TGGCTGGACCAATGTGAAC,
(Common Reverse): GTGTGACTGCATGACT AACTTTGA;
YAP-flox:
(Forward) CCGTTTCTCCTGGGACACTC,
(Reverse): CCACAAAAGTCTGCAAAAAGGC.

All the mice were kept under specific pathogen-free conditions and housed in a barrier facility in the Animal Department of our institute. All the animal experiments were performed in compliance with all relevant ethical guidelines approved by the Ethics Committee of Tianjin Medical University Cancer Institute and Hospital (HSTF-AE-2023003).

Cell lines
B16-F10 cells and HEK293T cells were maintained in Dulbecco's Modified Eagle's Medium with 10% fetal bovine serum and 1% penicillin-streptomycin. MC-38 cells were cultured in a complete RPMI 1640 medium. All cells were obtained from American Type Culture Collection and tested negative for mycoplasma contamination.

Tumor models and treatment
WT or cKO mice (n=5, 6–8 weeks) were inoculated with $3–5×10^5$ MC-38 cells/100 µl PBS, or $2×10^5$ B16–F10 melanoma cells/100 µl PBS on the right flank on day 0. Tumor growth was recorded every 1–2 days. Tumor volume was determined as length (mm)×width^2 (mm)×0.52.

β-Aminopropionitrile (BAPN) treatment

Mice were randomly assigned to groups treated with PBS or BAPN (100 mg/kg, intraperitoneally (I.P.), every 2 days; MCE)[20] on day 7 after MC-38 cell inoculation. All mice were sacrificed on day 21 for further study.

Verteporfin (VP) treatment and low leucine diet treatment

VP is a YAP inhibitor which disrupts YAP-TEA Domain Transcription Factor (TEAD) interactions.[21] VP (2 mg/mouse, I.P. every 2 days; MCE) was given every other day from day 7 until mice were sacrificed. A low leucine diet (10% content of leucine compared with normal chow) and compared normal diet (purchased from Jiangsu Xietong Pharmaceutical Bio-engineering) were provided on day 0 until mice sacrifice.

Masson staining and hydroxyproline assay
The tumor paraffin slices were stained using Masson staining kit (Solarbio) according to the manufactures protocol, collagen secretion was evaluated by the blue area. The content of hydroxyproline was measured by using hydroxyproline assay kit (Solarbio).

Flow cytometry
Single-cell suspensions were prepared from spleens or tumors. Tumor tissues were cut into pieces and digested in a mixture solution (1 mg/mL collagenase intravenously,

0.1 mg/mL hyaluronidase and 30 U/mL DNase I mixed in complete RPMI 1640 medium) at 37°C for 40 min with gentle agitation. The single-cell suspension was strained through 70 μm and 40 μm filters on ice. Spleens were smashed slightly on the strainers directly to get single cells. After red blood cell lysis (ACK lysing Buffer; Gibco), cells were blocked with anti-mouse CD16/32 antibodies. Zombie NIR or Aqua was used to distinguish dead and live cells, then a mixture of antibodies was incubated for about 30 min before washing. The intracellular marker staining was performed using a Foxp3/Transcription Factor Staining Buffer Set (Invitrogen) according to the manufacturer's instructions. For chemokine staining, cells were activated with an activation cocktail for 4 hours before permeabilization and fixation. Antibodies used in our experiments were listed in online supplemental table 2. Data were collected using BD FACSCanto II or Beckman CytoFLEX flow cytometers and analyzed in FlowJo V.10.

In vitro Treg cell assays

Treg isolation.

CD4⁺Foxp3-YFP⁺ Treg cells from spleen or TI lymph cells were sorted on a FACSAria III (BD Biosciences) in our institute and maintained in complete RPMI 1640 medium supplemented with IL-2 (100 IU/mL, PeproTech) and TGFβ (5 ng/mL, PeproTech) for further experiments.

Treg induction in vitro

For Treg induction, a naïve CD4⁺ T cells isolation kit (Miltenyi Biotec) was used to get the naïve CD4⁺ T cells from the spleens of 6–8 weeks old WT mice. Cells were cultured for 3 days in U-bottom 96-well plates in complement RPMI 1640 medium supplemented with IL-2 (100 IU/mL; PeproTech), TGFβ (5 ng/mL; PeproTech) and anti-CD3/28 Dynabeads (cells: Dynabeads=5:1; Gibco).

Plasmid, lentivirus construction and infection

The pLV-EF1α-mLars2-puro plasmid was purchased from Synbio Technologies (China). The Lars2 plasmid was co-transfected with psPAX2 and pMD2.G into HEK293T cells, lentivirus particles were concentrated before infecting Treg cells according to the instructions described previously.[18]

RNA isolation and real-time PCR

RNA from TI-Tregs was extracted using the TRIzol reagent (Invitrogen), and the SYBR Premix Ex Taq II (Takara) was used for real-time PCR (RT-PCT). The primer sequences used for RT-PCR were as follows:

Lars2-F: GTGGGAAAGACTAATTCCAGGG
Lars2-R: GCCAGAAGGGTATGGGAACAT
Actin-F: GTGACGTTGACATCCGTAAAGA
Actin-R: GCCGGACTCATCGTACTCC

RNA-sequencing

TI-Tregs from the MC-38 tumor were sorted on a flow cytometer, and resuspended in the lysis buffer immediately for further RNA extraction and library building. The library was quality-assessed before being sequenced using the Illumina NovaSeq 6000 sequencing platform (Paired end150) to generate raw reads. Differentially expressed genes (DEGs) were identified by DESeq2 with a cut-off value of log2|fold-change|>1 and *p*-adjust<0.05. The clusterProfiler was used to perform functional enrichment analysis for the annotated significant DEGs, the potential genes in identified modules based on gene ontology (GO) and Kyoto Encyclopedia of Genes and Genomes (KEGG) pathway categories. Terms with p<0.05 were considered significant. Gene set enrichment analysis (GSEA) was performed by the function in package clusterProfiler with a gene list sorted by log2 fold-change.

Luciferase assay and CHIP assay

A 2 kb DNA sequence of the *Lars2* promoter was cloned into PGL3.0-basic vector plasmid. HEK293T cells were transfected with various plasmids in different groups, including PGL3-basic, PGL3-control, PGL3-Lars2 promoter, pLV-YAP, pLV-TEAD1, and pRL-TK, for 24 hours. The Dual-Luciferase Reporter Assay System (Promega, E1910) was used to analyze the firefly and renilla luminescence following the manufacturer's protocol.

The CHIP (chromatin immunoprecipitation) assay was conducted using a CHIP assay kit according to the manufacturer's instructions. Quantitative PCR analysis was performed with the following primer sequences:

F'- TAGTTTATTCTGAGGCCACTAA
R'- TTTAACTGCTCTGGTGTC

Mitochondrial function assay

Fluorescent probes for mitochondrial staining.

Different probes were used to assess mitochondrial function according to the manufacturers' protocols. ATP-Red probe (MCE) and MitoTracker Red probe (Invitrogen) were used to evaluate ATP production and mitochondrial mass in Treg cells, respectively. MitoSOX Red probe (Invitrogen) was employed for examining the levels of reactive oxygen species (ROS) within mitochondria. BODIPY 558/568 C12 (Invitrogen) was used to test fatty acid absorption ability.

Seahorse assay.

TI-Tregs were sorted by flow cytometry from the MC-38 tumor, and then maintained in a complete RPMI 1640 medium supplemented with IL-2 (100 IU/mL; PeproTech), TGFβ (5 ng/mL; PeproTech) and anti-CD3/28 Dynabeads (cells: Dynabeads=3:1; Gibco) in U-bottom 96-well plate for about 12 hours before planting into 96-well Seahorse plates, which were previously coated with Cell-Tak (Corning) according to manufacturer's instructions. 2×10^5 cells were plated in 50 μl Seahorse RPMI medium supplemented with 2 mM glutamine, 10 mM glucose and 2 mM sodium pyruvate. Cells were incubated at 37°C without CO_2 for 20 min after centrifuging the plate at 200 g without a break. Afterward, 130 μl Seahorse RPMI medium was added to each well to bring the final

volume to 180 µl. The mito stress test was performed using XF96 Analyzer (Agilent) according to established protocols under basal conditions and also in response to 1 µM Oligomycin, 1 µM FCCP and 0.5 µM Rotenone/Antimycin (Agilent).

Transmission electron microscopy analysis

TI-Tregs were sorted from MC-38 tumors from WT and YAP-cKO mice using flow cytometry, then resuspended in 2.5% glutaraldehyde fixed solution overnight at 4°C. After dehydration, embedding in resin, and uranium acetate staining, slices were observed with the Hitachi transmission electron microscopy system (Japan).

Patients and clinical characteristics

106 patients with gastric cancer who received no treatments before surgery were recruited in this study. All patients enrolled in the study signed informed consents. Clinicopathological characteristics were collected and provided in online supplemental table 1. Overall survival (OS) was calculated from the time of surgery to the last follow-up or death.

Multiplex immunohistochemistry and multispectral analysis

Formalin-fixed and paraffin-embedded tumor samples were collected, and multiplex immunohistochemistry (mIHC) staining was carried out using an Opal 7-Color Manual IHC Kit (PerkinElmer, NEL811001KT) according to the manufacturer's instructions. CD4 was labeled by Opal 650, Foxp3 was labeled by Opal 570, YAP was labeled by Opal 520. Spectral resolution and phenotype analysis were conducted using Akoya inForm software. Visualization and quantitation were achieved using TissueFAXS SPECTRA systems and StrataQuest analysis (TissueGnostics), according to previously described methods.[22] The high and low YAP+ Treg groups were defined by the mean value of the YAP expression ratio in all patients.

Statistical analysis

Statistical analysis was performed using GraphPad Prism software V.9. Survival functions were performed by the Kaplan–Meier method with a log-rank test to compare survival between groups. One-way analysis of variance was used for multiple group comparisons. Unpaired or paired two-tailed Student's t-test was used for two different group comparisons. P value < 0.05 was considered statistically significant. ns, not significant; *p<0.05; **p<0.01; ***p<0.001. ****p<0.0001.

RESULTS

Matrix stiffness activated YAP in Treg

YAP was essential for Treg function through bolstering Foxp3 expression,[18] however, the reason for YAP activation in Treg still remains elusive. Given YAP's established role as a key mechanotransducer, we postulated that the mechanical signal emanating from the matrix in solid tumors could potentially activate YAP in TI-Tregs. We compared YAP expression in Treg cells from gastric tumor and normal gastric tissue, and found that TI-Tregs had more YAP expression (figure 1A). Furthermore, TI-Tregs derived from MC-38 tumors displayed higher YAP activation compared with those isolated from the spleen (figure 1B). To further validate our hypothesis, we used a hydrogel model to emulate the behavior of soft and stiff matrix following the method published before.[23] Tregs were induced from mouse naïve CD4+ T cells on hydrogel with varying stiffness (figure 1C). An enhancement in the efficiency of Treg induction was observed as the matrix stiffness increased (figure 1D), which was also accompanied by the activation of YAP (figure 1E). Foxp3 expression was significantly higher in YAP+CD4+ T cells compared with YAP− CD4+ T cells induced both on soft (figure 1F) and stiff hydrogel (online supplemental figure S1A).

To determine whether YAP mediated the mechanical signals from matrix stiffness in TI-Tregs in vivo, BAPN was administered to tumor-bearing mice after inoculation with MC-38 cancer cells. BAPN is a Lox enzyme inhibitor and it could inhibit matrix crosslinking to produce mice with more compliant tumors.[24] The effect of BAPN was confirmed by both Masson staining and hydroxyproline measurement (online supplemental figure S1B and S1C). As shown in the figure, BAPN efficiently inhibited tumor growth (figure 1G), which was in line with previous research that BAPN possessed the capability to suppress tumor progression.[25] As expected, YAP in TI-Tregs was decreased in BAPN-treated softer tumors (figure 1H). Infiltration of Treg cells was notably diminished in softer tumors (figure 1I), meanwhile, the immunosuppressive function was also compromised, including decreased expression of cytotoxic T-lymphocytes-associated protein 4 (CTLA-4), programmed cell death protein-1 (PD-1) (figure 1J) and a reduced percentage of CD44+CD62L− effector cells (online supplemental figure S1D). In comparison to stiff tumors, the percentage of infiltrating CD8+ T cells increased significantly in softer tumors (figure 1K). To further assess the functionality of CD8+ T cells, cytotoxic granule and cytokine secretion were examined. In softer tumors, CD8+ T cells exhibited a higher frequency of GZMB+CD8+ T cells, as well as a slightly higher frequency of TNFα+CD8+ T cells (figure 1L and online supplemental figure S1E). Differences in the frequencies of CD44+CD62L− effector cells among CD8+ T cells between the two groups were not obvious (online supplemental figure S1F). Taken together, we demonstrated the mechanical signals from a stiff matrix could activate YAP in Treg cells.

YAP deficiency impaired immunosuppressive capacity of TI-Treg

Having observed the activation of YAP in TI-Tregs on a stiff matrix, we then proceeded to evaluate its pivotal role in maintaining the immunosuppressive function of TI-Tregs. Foxp3cre YAPfl/fl mice (here indicated as YAP-cKO mice in our study) were generated in our lab. There were no significant differences between
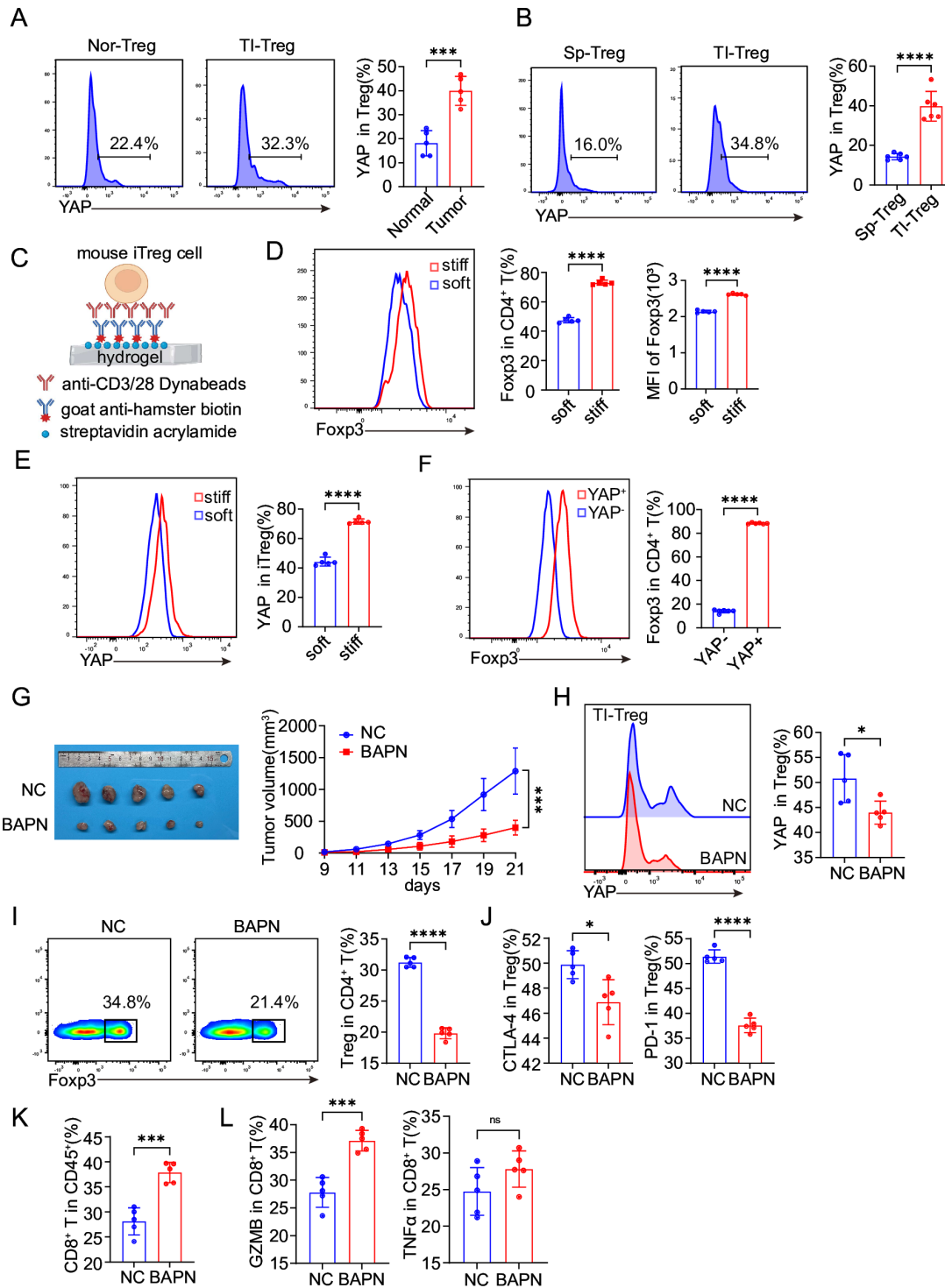
Figure 1 Matrix stiffness activates YAP in Treg. (A) Quantification of YAP in infiltrating Treg cells derived from stiff gastric tumors and soft normal gastric tissues (n=5 per group). (B) Quantification of YAP in Treg cells derived from tumors and spleens of MC-38 tumor-bearing WT mice (n=6 per group). (C) A schematic figure of inducting Treg system on different stiff hydrogel in vitro. (D) Percentage and MFI of Foxp3 in CD4$^+$ T cells induced on soft and stiff matrix. (E) Percentage of YAP in iTreg cells induced on soft and stiff matrix. (F) Percentage of Foxp3 in YAP$^+$ and YAP$^-$ CD4$^+$ T cells induced on soft matrix. (G–H) Soft and stiff tumor matrix models were constructed in vivo using BAPN and PBS treatments, respectively. (G) Tumor growth of MC-38 cells bearing WT mice administrated with PBS (NC) or BAPN (100 mg/kg, I.P., every 2 days) (n=5 per group). (H) Representative flow plot and percentage of YAP$^+$ cells among the TI-Tregs. (I) Representative flow plots and percentage of TI-Tregs among intratumor CD4$^+$ T cells. (J) Percentage of CTLA-4$^+$ and PD-1$^+$ cells in TI-Tregs. (K) Percentage of CD8$^+$ T cells among CD45$^+$ cells. (L) Percentage of GZMB$^+$ and TNFα^+ cells in CD8$^+$ T cells. The data were presented as the mean±SD. ns, not significant; *p<0.05 ; **p<0.01; ***p<0.001.****p<0.0001. BAPN, β-Aminopropionitrile; CTLA-4, cytotoxic T-lymphocytes-associated protein 4; I.P., intraperitoneal; iTreg, inducted regulatory T cell; MFI, mean fluorescence intensity; NC, negative control; PBS, phosphate-buffered saline; PD-1, programmed cell death protein-1; TI-Tregs, tumor-infiltrating regulatory T cells.
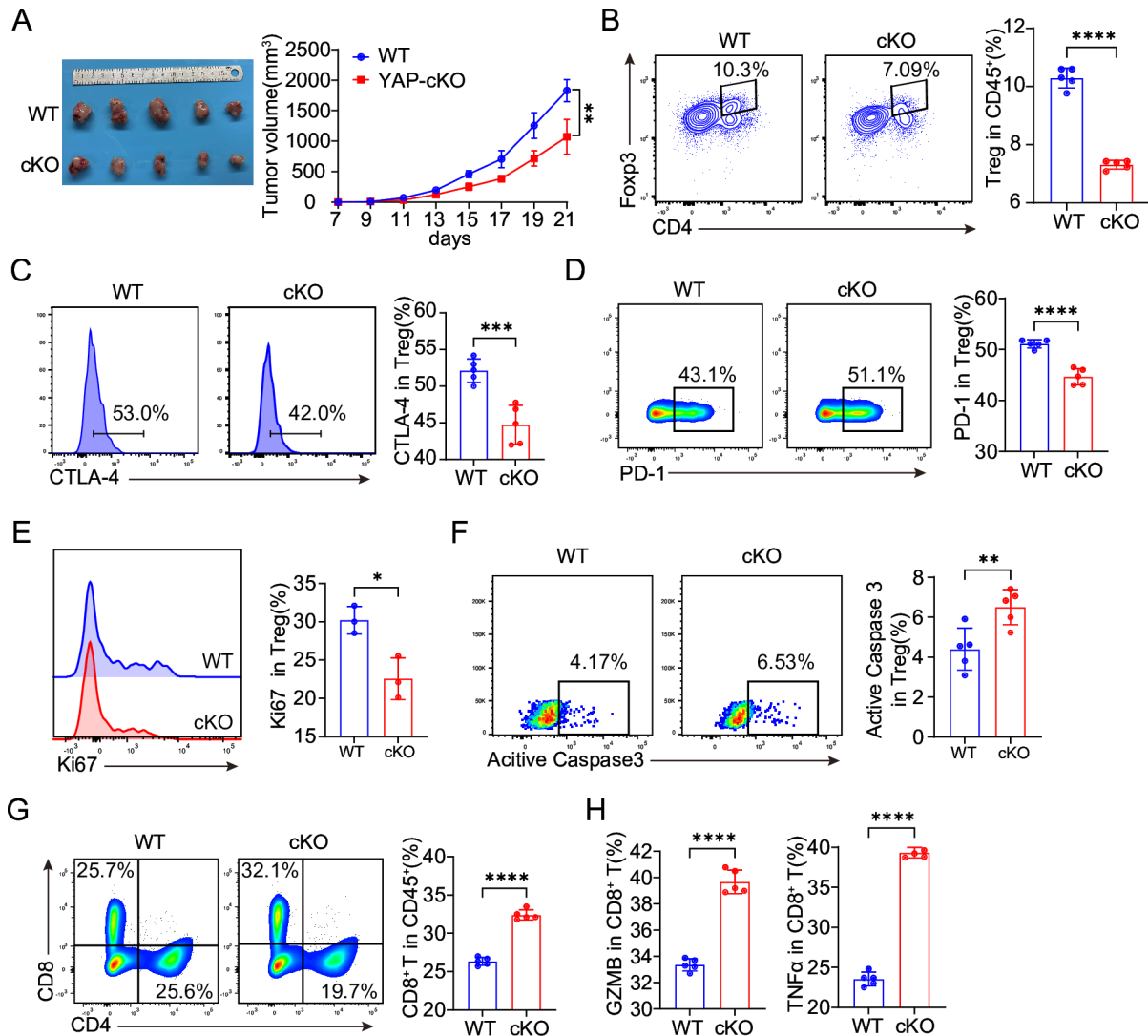
Figure 2 YAP deficiency impaired immunosuppressive capacity of TI-Treg. (A) Tumor growth in WT and YAP-cKO mice challenged with MC-38 cancer cells (5×10^5 cells per mouse, n=5 per group). (B) Percentage of TI-Tregs among CD45$^+$ cells. (C–F) Representative flow plots and tabulated percentages of CTLA-4$^+$ cells (C), PD-1$^+$ cells (D), Ki67$^+$ cells (E) and active caspase 3$^+$ cells (F) in TI-Tregs. (G) Percentage of intratumor CD8$^+$ T and CD4$^+$ T cells among CD45$^+$ cells. (H) GZMB$^+$ and TNFα$^+$ cells among CD8$^+$ T cells. The data were presented as the mean±SD. ns, not significant; *p<0.05 ; **p<0.01; ***p<0.001. ****p<0.0001. CTLA-4, cytotoxic T-lymphocytes-associated protein 4; PD-1, programmed cell death protein-1; TI-Treg, tumor-infiltrating regulatory T cell.

WT and YAP-cKO mice in either appearance or body weight (online supplemental figure S2A), nor in the appearance of the spleen in non-tumor-bearing mice (online supplemental figure S2B). Meanwhile, there was no difference in the ratios of CD4$^+$, CD8$^+$, and Treg cells among CD45$^+$ cells isolated from the spleen (online supplemental figure S2C), which was in line with the results of Ni *et al.*[18] Cancer cells were inoculated into *Foxp3*^{cre} mice (here indicated as WT mice in our study) and YAP-cKO mice, in order to construct the tumor-bearing model. Notably, in comparison to WT mice, tumor growth was significantly suppressed in YAP-cKO mice, evident both in MC-38 and in B16-F10 tumor-bearing models (figure 2A and online supplemental figure S3A). The frequencies of TI-Tregs infiltration decreased (figure 2B and online supplemental

figure S3B), along with a reduction in CTLA-4 and PD-1 expression (figure 2C and figure 2D), suggesting a compromise in their immunosuppressive function. Moreover, the deficiency of YAP in TI-Tregs diminished their proliferation and increased their susceptibility to apoptosis (figure 2E and F). The infiltration of CD8$^+$ T cells increased (figure 2G), along with elevated secretions of GZMB and TNFα (figure 2H and online supplemental figure S3C). Additionally, a significant elevation in the proportion of CD44$^+$CD62L$^-$ effector cells among CD8$^+$ T cells was observed in YAP-cKO mice (online supplemental figure S3D). Immunosuppressive cells, such as myeloid-derived suppressor cells, M2-like tumor-associated macrophages were also downregulated in YAP-cKO mice (online supplemental figure S3E and F). Collectively, the deficiency of YAP in TI-Tregs impaired

their immunosuppressive function and activated the immune environment within the tumor.

YAP was essential for the maintenance of mitochondrial function in TI-Treg

To decipher the underlying mechanism of how YAP regulates the immunosuppressive function of TI-Tregs, we conducted RNA-Seq analysis on TI-Tregs isolated from WT and YAP-cKO MC-38 tumor-bearing mice. We identified a total of 876 DEGs between YAP-cKO and WT TI-Tregs, which included 800 downregulated versus 76 upregulated DEGs as shown in the volcano plot (figure 3A and online supplemental figure S4A). GO analysis of these DEGs revealed that cellular metabolic processes, specifically mitochondrial OXPHOS, were enriched in the biological process subgroup, whereas protein translation was enriched in both the molecular function (MF) and cellular component subgroups (figure 3B). KEGG enrichment revealed that a variety of pathophysiological processes were involved following YAP knockout in TI-Tregs (online supplemental figure S4B). Among those, OXPHOS was highly enriched in the metabolic pathway enrichment. The enrichment of the Hippo pathway, cell adhesion molecules, and regulation of the actin cytoskeleton reflected the quality of the sequencing data given the MF of YAP. Furthermore, the TGFβ pathway was disrupted in YAP-cKO TI-Tregs, which was consistent with previous studies.[18] GSEA analysis showed a decrease in aerobic respiration (figure 3C) and T cell activation (online supplemental figure S4C) in YAP-cKO TI-Tregs. All these findings suggest a potential association between YAP and mitochondrial OXPHOS in TI-Tregs.

To further validate the crucial role of YAP in regulating mitochondrial function in TI-Tregs, we initially assessed ATP levels in WT and YAP-cKO TI-Tregs. Notably, our analysis revealed a significant decline in ATP production in YAP-deficient TI-Tregs (figure 3D). Concurrently, we observed a decrease in mitochondrial mass in TI-Tregs derived from MC-38 tumors and B16-F10 tumors (figure 3E and online supplemental figure S4D). The mitochondrial respiratory chain is the central generator of energy production as well as the predominant source of intracellular ROS, which is the byproduct of electron transfer.[26] Therefore, we compared mitochondrial ROS levels and discovered that YAP-cKO Tregs exhibited lower mitochondrial ROS levels compared with WT ones, which indicated the dysfunction of respiratory chain complexes (figure 3F). To further quantify mitochondrial respiration, we conducted a mito stress test using seahorse analysis. The mitochondria in YAP-cKO TI-Tregs were found to be more incompetent, exhibiting diminished basal respiration, maximal mitochondrial respiration, and spare respiratory capacity (figure 3G), thus indicating mitochondrial dysfunction. We also checked mitochondrial morphology, finding that a heightened degree of vacuolation accompanied by the disappearance of ridges, as well as a higher frequency of mitophagy in YAP-cKO TI-Tregs (figure 3H). The morphology of mitochondria

further confirmed mitochondrial dysfunction in YAP-cKO TI-Tregs.

As OXPHOS is the main energy resource sustaining TI-Tregs' function,[27] which could be fueled by a variety of substrates, such as fatty acid.[28] We tested fatty acid absorption and found a significant decrease in BODIPY C12 absorption in YAP-cKO TI-Treg (online supplemental figure S4E). Insufficient energy intake provides further evidence to support the existence of mitochondrial dysfunction. Based on these findings, we concluded that YAP deficiency leads to mitochondrial dysfunction in TI-Tregs, thereby compromising their immunosuppressive capabilities.

YAP enhanced mitochondrial function by regulating *Lars2* transcription

Mitochondrial morphology, structures, mass and even quantity exhibit high plasticity under the regulation of certain molecules in different environment.[29] In order to uncover the molecular mechanism YAP regulating mitochondrial function, we compared the top 50 down DEGs between WT and YAP-cKO TI-Treg, finding that *Lars2* was the most candidate gene related to mitochondrial dysfunction (figure 4A).

Lars2, which is responsible for mitochondrial gene translation, may have an affection on genes related to mitochondrial respiratory chain complexes I–V.[30] GSEA analysis revealed that mitochondrial protein-containing complex was downregulated in YAP deficient TI-Tregs (online supplemental figure S5A), and genes related to mitochondrial respiratory chain complexes were also downregulated, as shown in the heatmap (online supplemental figure S5B). Since YAP functions as a mechanosensitive transcriptional cofactor that enhances TEAD to regulate gene transcription,[31] we found that *Lars2* messenger RNA (mRNA) was significantly downregulated in YAP-cKO TI-Tregs (figure 4B). Furthermore, we observed a reduction in both mean fluorescence intensity and the percentage of Lars2 protein in these YAP-cKO TI-Tregs (figure 4C). Multiple TEAD-binding sites were identified in the Lars2 promoter, luciferase assay revealed that binding site located at −211~−202 bp (figure 4D), and this site was further confirmed by CHIP-qPCR (figure 4E). Collectively, we confirmed that *Lars2* transcription could be regulated by YAP.

However, it was still unclear whether mechanical signals could upregulate Lars2 through YAP. Given that tumors are stiffer than the spleen, we compared Lars2 expression in Treg cells derived from the spleen and tumor in MC-38 tumor-bearing mice. Notably, TI-Tregs displayed a higher expression of Lars2 at both mRNA and protein levels (figure 4F and figure 4G). When cultured on a stiff matrix, iTreg cells expressed more Lars2 compared with those cultured on the soft matrix (figure 4H). Additionally, the expression of Lars2 was significantly higher in YAP+ iTreg cells than in YAP− iTreg cells cultured on a stiff matrix (figure 4I). All the evidence indicated that YAP mediated the regulation of Lars2 in response to mechanical signals. Furthermore, the effects
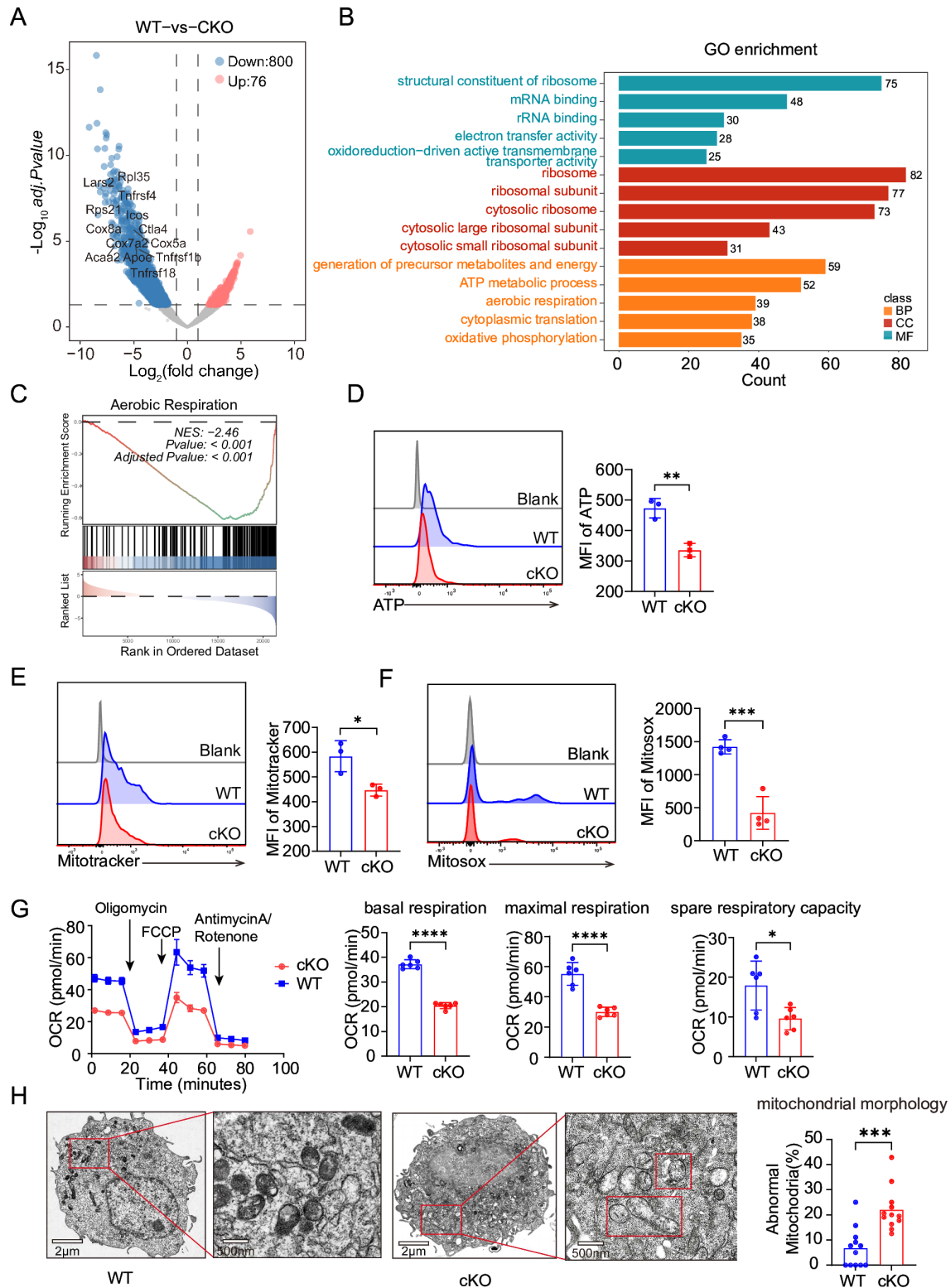
Figure 3 YAP was essential for the maintenance of mitochondrial function in TI-Treg. (A–C) TI-Tregs were isolated from MC-38 tumors in WT and YAP-cKO mice for RNA-seq (n=3 per group). (A) Volcano plot showing DEGs, and the most significant genes were labeled in the graph. (B) GO enrichment analysis of DEGs. (C) Genes related to aerobic respiration were enriched in GSEA analysis. (D–H) Mitochondrial function and morphology were compared between WT and YAP-cKO TI-Tregs derived from MC-38 tumors. Representative flow plots and tabulated differences of ATP production (D), mitochondrial mass (labeled by MitoTracker) (E), mitochondrial superoxide accumulation (labeled by MitoSOX) in TI-Tregs. (G) Assessment of mitochondrial stress in TI-Tregs using seahorse assay. (H) Representative TEM images and tabulated differences of mitochondria in TI-Tregs. The data were presented as the mean±SD. ns, not significant; *p<0.05; **p<0.01; ***p<0.001.****p<0.0001. DEGs, differentially expressed genes; GO, gene ontology; GSEA, gene set enrichment analysis; MFI, mean fluorescence intensity; TEM, transmission electron microscopy; TI-Tregs, tumor-infiltrating regulatory T cells.
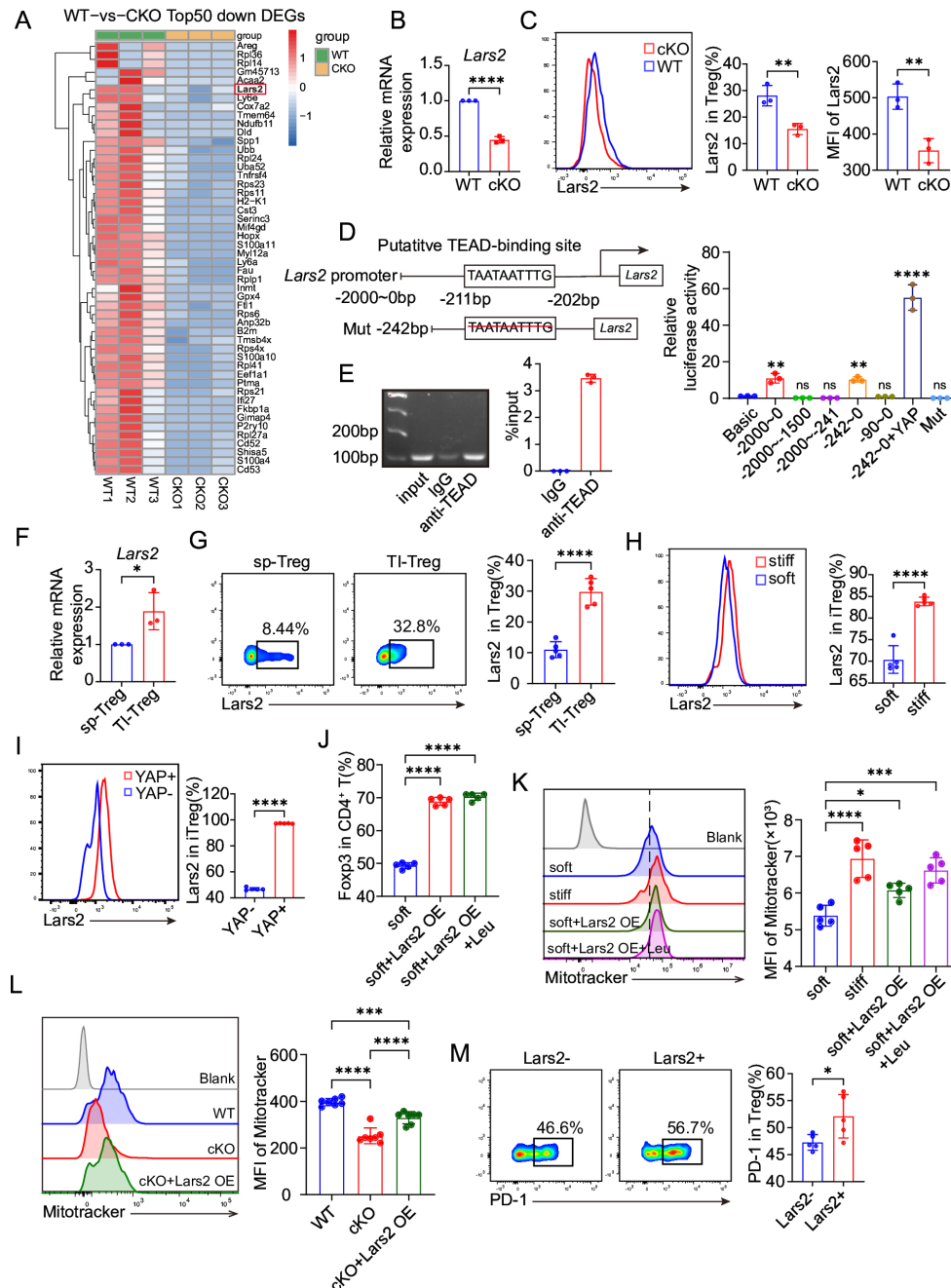
Figure 4 YAP enhanced mitochondrial function by regulating *Lars2* transcription. (A) Top 50 downregulated DEGs in WT and YAP-cKO TI-Tregs. (B, C) Relative *Lars2* mRNA and protein expression in TI-Tregs. (D) Schematic of putative TEAD binding site and a luciferase reporter constructed with mutation (deleting the binding site) on the *Lars2* promoter. Luciferase activity in HEK293T cells transfected with indicated plasmids. (E) CHIP assay performed in HEK293T cells. (F, G) Relative *Lars2* mRNA and protein expression in Treg cells derived from spleens and tumors from MC-38 tumor bearing mice. (H–K) Induction of Treg cells from mouse naïve CD4⁺ T cells on soft or stiff matrix in vitro under indicated treatments. (H) Representative flow plots and tabulated percentage of Lars2 in iTreg cells induced on soft and stiff matrix. (I) Representative flow plots and tabulated percentage of Lars2 in YAP⁺ and YAP⁻ iTreg cells induced on stiff matrix. (J) Percentage of Foxp3 in CD4⁺ T cells induced by culturing on a soft matrix, with or without lentiviral-mediated overexpression of Lars2, and simultaneously supplementing with leucine (1 mM) for 48 hours. (K) Representative flow plots and tabulated differences of mitochondrial mass (labeled by MitoTracker) in iTreg cells in indicated groups (soft matrix, stiff matrix, soft matrix+overexpression of Lars2 with lentivirus, soft matrix+overexpression of Lars2 with lentivirus+leucine (1 mM)). (L) Representative flow plots and tabulated differences of mitochondrial mass (labeled by MitoTracker) in Treg cells derived from spleen cultured on stiff matrix under indicated treatments (WT Treg, YAP-cKO Treg, YAP-cKO Treg+overexpression of Lars2 with lentivirus). (M) Representative flow plots and tabulated percentage of PD-1 in Lars2⁺ and Lars2⁻ TI-Tregs. The data were presented as the mean±SD. ns, not significant; *p<0.05; **p<0.01; ***p<0.001. ****p<0.0001. CHIP, chromatin immunoprecipitation; DEGs, differentially expressed genes; iTregs, induced Treg cells; Lars2, leucyl-tRNA synthetase 2, mitochondrial; MFI, mean fluorescence intensity; mRNA, messenger RNA; TEAD,TEA domain transcription factor; PD-1, programmed cell death protein-1; TI-Tregs, tumor-infiltrating regulatory T cells.

of Lars2 in regulating mitochondrial function in Treg cells were evaluated. Overexpression of Lars2 or supplementing leucine (the substrate amino acid of Lars2) at the same time elevated iTreg cells induction efficiency on the soft matrix (figure 4J and online supplemental figure S5C). The mitochondrial mass was compared among the indicated groups (figure 4K), iTreg cells cultured on a stiff matrix displayed the highest mitochondrial mass, indicating that mechanical stimuli enhanced mitochondrial function effectively. Lars2 overexpression or adding leucine concurrently elevated mitochondrial mass in iTreg cells. YAP inhibitor, VP, was able to decrease mitochondrial function in iTreg cells cultured on stiff matrix (online supplemental figure S5D). Furthermore, Lars2 overexpression partially rescued mitochondrial dysfunction in YAP-cKO Treg cells cultured on a stiff matrix in vitro (figure 4L). It was also found that Lars2$^+$ TI-Tregs had more PD-1 expression, indicating that they possessed a stronger immunosuppressive ability (figure 4M). Overall, the collective results suggested that YAP enhanced mitochondrial function in TI-Tregs by upregulating *Lars2* transcription in response to mechanical signals.

Low leucine diet impaired mitochondrial function in TI-Treg

Lars2 was an enzyme synthesizing mitochondrial leucyl-tRNA responsible for maintaining mitochondrial function, its functionality strongly depended on the substrate leucine,[32] so lowering leucine intake might compromise TI-Tregs immunosuppressive function. After tumor inoculation, mice were provided with either a normal or a low leucine diet, and the tumor growth was subsequently evaluated between the two groups. A low leucine diet slightly slowed down the tumor growth compared with a standard diet (figure 5A). The frequency of TI-Tregs decreased in the low leucine diet group (figure 5B), and so did CTLA-4$^+$ cells in TI-Tregs (figure 5C). Interestingly, Lars2 in TI-Tregs was increased in low leucine diet group (figure 5D), which might be the feedback effect in order to adjust to the low substrate supply. Inadequate leucine consumption by TI-Tregs led to a diminution in mitochondrial mass (figure 5E), as well as a decrease in ATP production (figure 5F). As the immunosuppressive function of TI-Tregs compromised, the frequency of CD8$^+$ T cells substantially increased (online supplemental figure S6A), and CD8$^+$ T cells became more productive in TNFα secretion (online supplemental figure S6B). Furthermore, the frequency of CD44$^+$CD62L$^-$ effector cells among CD8$^+$ T cells were also slightly elevated (online supplemental figure
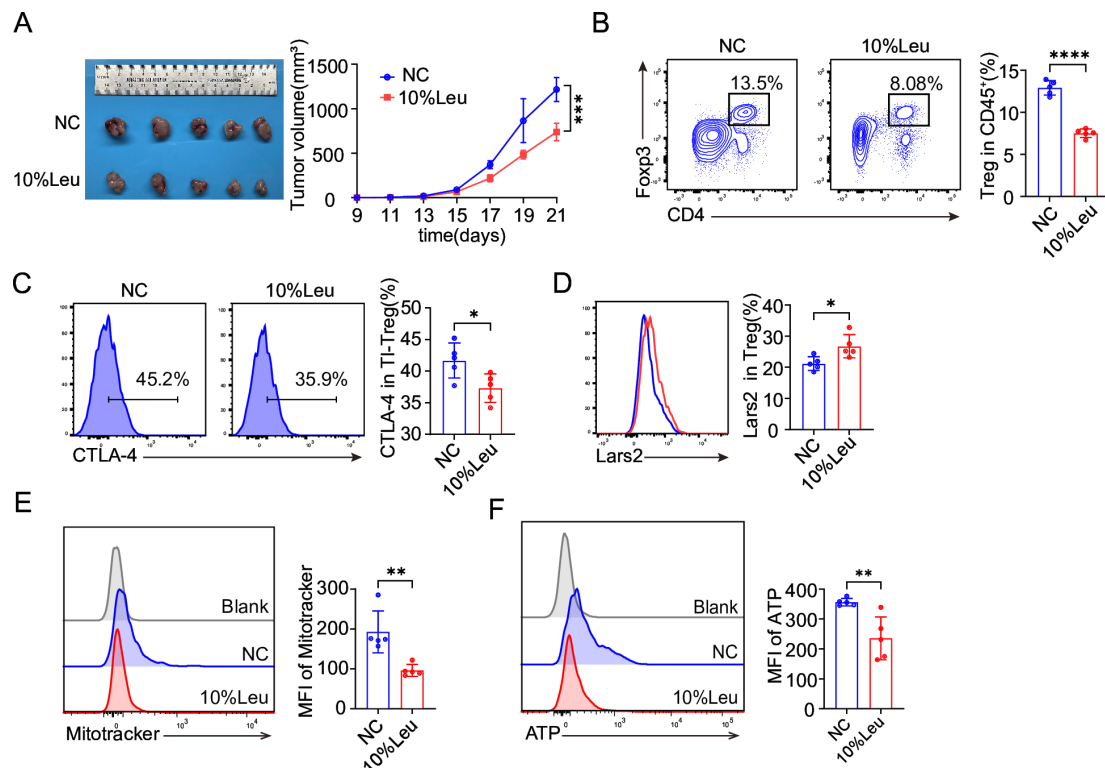

Figure 5 Low leucine diet impaired mitochondrial function in TI-Treg. WT and YAP-cKO mice were challenged with MC-38 cancer cells (5×10^5 cells per mouse, n=5 per group) on day 0. 10% leucine diet (10% content of leucine compared with normal chow) and compared normal diet (NC) were provided from day 0 to day 21 until mice were sacrificed. (A) Tumor growth of WT and YAP-cKO mice fed with different diets. (B) Representative flow plots and the percentage of TI-Tregs among CD45$^+$ cells. (C, D) Representative flow plots and tabulated percentages of CTLA-4$^+$ cells (C), Lars2$^+$ cells (D) in TI-Tregs. (E, F) Representative flow plots and tabulated differences of mitochondrial mass (labeled by MitoTracker) (F) and ATP production (E) in TI-Tregs. The data were presented as the mean±SD. ns, not significant; *p<0.05; **p<0.01; ***p<0.001. ****p<0.0001. CTLA-4, cytotoxic T-lymphocytes-associated protein 4; Lars2, leucyl-tRNA synthetase 2, mitochondrial; MFI, mean fluorescence intensity; NC, negative control; TI-Tregs, tumor-infiltrating regulatory T cells.
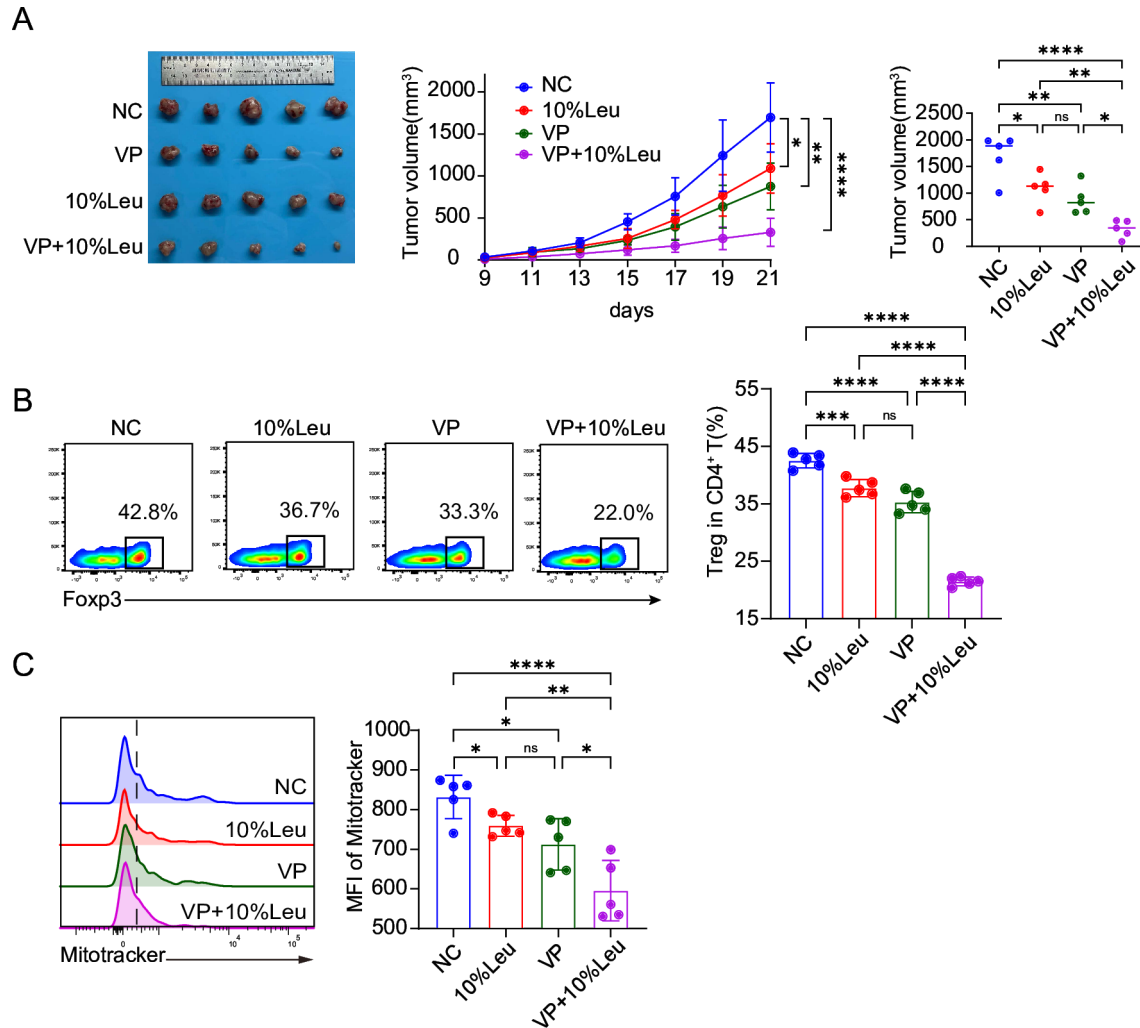
Figure 6 Combined YAP inhibition and low leucine diet synergistically suppressed tumor growth by disrupting TI-Tregs mitochondria. WT mice were challenged with MC-38 cancer cells (5×10^5 cells per mouse, n=5 per group) on day 0, 10% leucine diet (10% content of leucine compared with normal chow) and compared normal diet (NC) was provided from day 0 to day 21 until mice were sacrificed. VP (2 mg/mice, I.P., every 2 days) was administered on day 7 to the VP group and VP+10% Leu group until mice sacrifice. (A) Tumor growth and tumor volume of WT mice in the indicated groups. (B) Representative flow plots and percentage of TI-Tregs among CD45$^+$ cells. (C) Representative flow plots and tabulated differences in mitochondrial mass (labeled by MitoTracker) in TI-Tregs. The data were presented as the mean±SD. ns, not significant; *p<0.05; **p<0.01; ***p<0.001. ****p<0.0001. I.P., intraperitoneal; MFI, mean fluorescence intensity; NC, negatitve control; TI-Tregs, tumor-infiltrating regulatory T cells; VP, verteporfin.

S6C). These data revealed that a low leucine diet-induced insufficiency in Lars2 function could lead to mitochondrial dysfunction in TI-Tregs, subsequently compromising their immunosuppressive activity.

Combined YAP inhibition and low leucine diet synergistically suppressed tumor growth by disrupting TI-Tregs mitochondria

Since YAP and Lars2 were critical in sustaining TI-Tregs function, we explored the potential benefits of integrating YAP inhibition with low leucine diet adjustment in anti-tumor therapy. Tumor growth curve and tumor volume were plotted for MC-38 tumor-bearing mice treated with various regimens. Among them, the combination of VP and low leucine diet was the most effective in inhibiting tumor growth (figure 6A), with the most significant decrease in the infiltration of TI-Tregs (figure 6B). The assessment of

mitochondrial function revealed a significant reduction in mitochondrial mass in TI-Tregs within the combining group (figure 6C). Based on the data above, we concluded that a diet with low leucine intake could enhance the antitumor effect of YAP inhibitors by compromising mitochondrial function of TI-Treg cells.

High YAP$^+$ TI-Treg infiltration predicted poor prognosis in patients with gastric cancer

Gastric cancer was the third leading cause of cancer-related death worldwide,[33] and it is also the most frequently encountered solid tumor among patients. Based on the aforementioned results, we compared the expression of Lars2 in Tregs derived from fresh gastric tumor (stiff) and normal gastric tissue (soft). TI-Tregs expressed more Lars2 than Tregs derived from normal

gastric tissue, furthermore, Lars2 expression in YAP[+] TI-Tregs was significantly higher than in the YAP[−] subpopulation (figure 7A). This finding provides compelling evidence that matrix stiffness activates YAP and subsequently upregulates Lars2 expression in TI-Tregs in gastric cancer. In order to evaluate the predictive role of YAP[+] TI-Tregs in gastric cancer, we collected 106 tumor samples from patients with gastric cancer and subsequently conducted a mIHC analysis. Representative images are presented in figure 7B. Patients were categorized into high and low YAP[+] Treg groups, based on the median expression level of YAP in TI-Tregs. The correlations between high YAP[+] Tregs infiltration and clinical characteristics were analyzed in online supplemental table 1). Unfortunately, we did not find any significance in the relationship between Tregs or YAP[+] Tregs infiltration and those clinical characteristics (p>0.05), this might be due to the small sample size. However, OS was much worse among patients with high Treg infiltration in gastric cancer, particularly those exhibiting high YAP[+] Treg infiltration (figure 7C and figure 7D). In summary, high YAP[+] Treg infiltration could potentially serve as a prognostic marker for poor survival in patients with gastric cancer, nonetheless, this patient group might derive benefit from a combination of VP and a low leucine diet adjustment.

DISCUSSION

Mechanical cues in the TME could regulate cell morphology, behaviors and metabolism, including those of immune cells. Understanding the interplay between mechanical forces and immune cell behaviors is essential for developing effective solid cancer therapies.[34] Here in our study, we have shown that YAP in TI-Tregs acts as a mechanotransducer activated by matrix stiffness, which facilitates the immunosuppressive function of TI-Tregs by enhancing mitochondrial activity. Moreover, mIHC analysis confirmed that high YAP[+] Tregs infiltration is related to poorer survival in gastric cancer. Our work offers a novel insight into how the mechanical properties of TME influence the metabolic pattern of TI-Tregs.

It is reported that human Treg induction in vitro can be influenced by mechanical stiffness, yet the results remain elusive. Shi et al observed enhanced Treg induction on softer materials,[35] whereas another study found that Treg induction increased with greater material stiffness.[23] One reasonable explanation for these opposite conclusions might be the difference in the stiffness of the induction matrix, which varies from 140kPa to 2600kPa at most in these studies. Considering all these results are from human iTreg cells cultured in vitro, the impact of the mechanical signals applied by TME on TI-Tregs remains unknown. We thoroughly investigate this issue, both in vivo and in vitro, and uncover that TI-Tregs adapt to stiff TME through the activation of YAP, which subsequently boosts their mitochondrial function.

Cells can sense the mechanical force of their environment, and this intricate process is typically orchestrated by the synergistic action of ion channels, cell membrane receptors, and intricate intracellular signaling pathways. Piezo1 selectively restrains Treg cells, without influencing activation events or effector T cell functions.[36] We did notice from our RNA-seq data that some adhesion receptors, such as integrin, had changed in YAP-cKO TI-Treg. However, it still needs to be verified whether these changes are vital in mediating mechanosignal transduction.

Intrinsic and extrinsic mechanical properties regulate cellular activities not only in solid tumors but also in hematology diseases. Biochemical cues such as matrix stiffness could modulate multiple capacities of hematopoietic stem cells (HSCs) through mechanotransduction.[37] Hu et al reported that Ptpn21 played an important role in retaining HSCs within the bone marrow niche through a biomechanical mechanism.[38]

Mitochondria are at the heart of metabolic programs which are critical in determining cell state by providing necessary energy and molecular precursors for cellular functions,[39] thus making them the central target of metabolic regulation.[40] External physical and mechanical cues can directly entail metabolic changes through mitochondria modulation.[41] Mitochondrial OXPHOS depends on the function of the respiratory chain complex. Lars2 is involved in the translation of mitochondrial-related proteins, including the electron transport chain protein complex.[30] In this study, we uncover that the mechanoresponsive activation of YAP in TI-Tregs is crucial in upregulating Lars2 expression, which is essential for maintaining mitochondrial activity.

Moreover, mitochondria are central for nutrient sensing and metabolism, which indicates that nutrition is an important factor in mitochondrial dysfunction and disease.[39] Leucine, an essential amino acid, is a key component used by Lars2 as a substrate amino acid. In our research, we have demonstrated that a low leucine diet directly triggers mitochondrial dysfunction in TI-Tregs, stemming from the inhibition of Lars2 function. Consequently, personalized dietary plans for patients with tumor are poised to become vital tools in cancer therapy.

CONCLUSIONS

In summary, our study showed that YAP deficiency in TI-Tregs impairs mitochondrial function, thus hampering its immunosuppressive capacity and boosting antitumor immunity. Mechanistically, YAP increases *Lars2* transcription, which is essential for mitochondrial protein translation. Lars2 heavily depends on its substrate amino acid, leucine; therefore, lowering leucine intake decreases mitochondrial activity in TI-Tregs. This mechanism deepens our understanding of mechanical signals regulating mitochondrial activity in TI-Tregs, making diet adjustment combined with traditional medicine a promising strategy for tumor therapy.
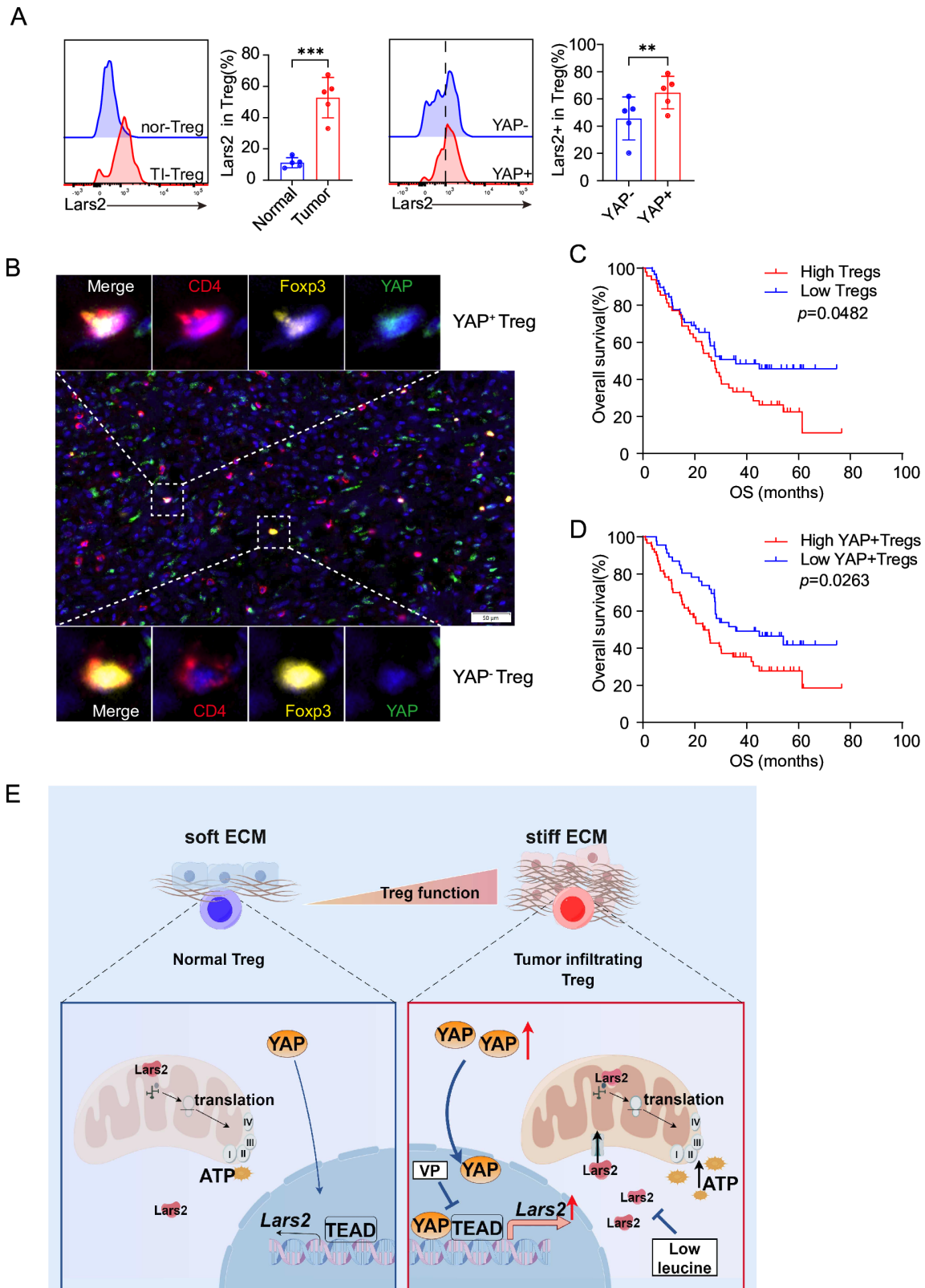
Figure 7 High YAP+ TI-Treg infiltration predicted poor prognosis in patients with gastric cancer. (A) Percentage of Lars2 in infiltrating Treg derived from fresh gastric cancer and normal gastric tissue samples (n=5 per group). Percentage of Lars2 in YAP+ and YAP− TI-Tregs derived from gastric cancer samples (n=5). (B) Representative mIHC images of gastric cancer samples. (C and D) Overall survival analysis of patients with gastric cancer based on total Treg infiltration level and YAP+ Treg infiltration level, respectively. High Treg infiltration and high YAP+ Treg infiltration were defined by the mean value. (E) The schematic diagram of the potential mechanism in this study. The data were presented as the mean±SD. ns, not significant; *p<0.05; **p<0.01; ***p<0.001. ****p<0.0001. ECM, extracellular matrix; Lars2, leucyl-tRNA synthetase 2, mitochondrial; mIHC, multiplex immunohistochemistry; TI-Tregs, tumor-infiltrating regulatory T cells; TEAD,TEA domain transcription factor.

ORCID iDs
Jingchao Bai http://orcid.org/0009-0002-5418-5461
Yuhan Zhang http://orcid.org/0000-0002-8511-4562

REFERENCES

1. Shan F, Somasundaram A, Bruno TC, *et al*. Therapeutic targeting of regulatory T cells in cancer. *Trends Cancer* 2022;8:944–61.
2. Kondo M, Kumagai S, Nishikawa H. Metabolic advantages of regulatory T cells dictated by cancer cells. *Int Immunol* 2024;36:75–86.
3. Watson MJ, Vignali PDA, Mullett SJ, *et al*. Metabolic support of tumour-infiltrating regulatory T cells by lactic acid. *Nature New Biol* 2021;591:645–51.
4. Yan Y, Huang L, Liu Y, *et al*. Metabolic profiles of regulatory T cells and their adaptations to the tumor microenvironment: implications for antitumor immunity. *J Hematol Oncol* 2022;15:104.
5. Shan Y, Xie T, Sun Y, *et al*. Lipid metabolism in tumor-infiltrating regulatory T cells: perspective to precision immunotherapy. *Biomark Res* 2024;12:41.
6. Fang Y, Zhang Q, Lv C, *et al*. Mitochondrial fusion induced by transforming growth factor-β1 serves as a switch that governs the metabolic reprogramming during differentiation of regulatory T cells. *Redox Biol* 2023;62:102709.
7. Jiang Y, Zhang H, Wang J, *et al*. Targeting extracellular matrix stiffness and mechanotransducers to improve cancer therapy. *J Hematol Oncol* 2022;15:34.
8. Du H, Bartleson JM, Butenko S, *et al*. Tuning immunity through tissue mechanotransduction. *Nat Rev Immunol* 2023;23:174–88.
9. Liu C, Li M, Dong Z-X, *et al*. Heterogeneous microenvironmental stiffness regulates pro-metastatic functions of breast cancer cells. *Acta Biomater* 2021;131:326–40.
10. Romani P, Nirchio N, Arboit M, *et al*. Mitochondrial fission links ECM mechanotransduction to metabolic redox homeostasis and metastatic chemotherapy resistance. *Nat Cell Biol* 2022;24:168–80.
11. Zheng Y, Zhou R, Cai J, *et al*. Matrix Stiffness Triggers Lipid Metabolic Cross-talk between Tumor and Stromal Cells to Mediate Bevacizumab Resistance in Colorectal Cancer Liver Metastases. *Cancer Res* 2023;83:3577–92.
12. Khalil AA, Smits D, Haughton PD, *et al*. A YAP-centered mechanotransduction loop drives collective breast cancer cell invasion. *Nat Commun* 2024;15:4866.
13. Patterson MR, Cogan JA, Cassidy R, *et al*. The Hippo pathway transcription factors YAP and TAZ play HPV-type dependent roles in cervical cancer. *Nat Commun* 2024;15:5809.
14. Lebid A, Chung L, Pardoll DM, *et al*. YAP Attenuates CD8 T Cell-Mediated Anti-tumor Response. *Front Immunol* 2020;11:580.
15. Meng KP, Majedi FS, Thauland TJ, *et al*. Mechanosensing through YAP controls T cell activation and metabolism. *J Exp Med* 2020;217:e20200053.
16. Mai Z, Lin Y, Lin P, *et al*. Modulating extracellular matrix stiffness: a strategic approach to boost cancer immunotherapy. *Cell Death Dis* 2024;15:307.
17. Wang J, Zhang B, Chen X, *et al*. Cell mechanics regulate the migration and invasion of hepatocellular carcinoma cells via JNK signaling. *Acta Biomater* 2024;176:321–33.
18. Ni X, Tao J, Barbi J, *et al*. YAP Is Essential for Treg-Mediated Suppression of Antitumor Immunity. *Cancer Discov* 2018;8:1026–43.
19. Shi LT, Lim JY, Kam LC. Substrate stiffness enhances human regulatory T cell induction and metabolism. *Biomaterials* 2023;292:121928.
20. Saatci O, Kaymak A, Raza U, *et al*. Targeting lysyl oxidase (LOX) overcomes chemotherapy resistance in triple negative breast cancer. *Nat Commun* 2020;11:2416.
21. Jiang Y, Fu L, Liu B, *et al*. YAP induces FAK phosphorylation to inhibit gastric cancer cell proliferation via upregulation of HMGB1. *Int J Biol Macromol* 2024;262:130037.
22. Luo J, Pang S, Hui Z, *et al*. Blocking Tim-3 enhances the anti-tumor immunity of STING agonist ADU-S100 by unleashing CD4$^+$ T cells through regulating type 2 conventional dendritic cells. *Theranostics* 2023;13:4836–57.
23. Shi L, Lim JY, Kam LC. Substrate stiffness enhances human regulatory T cell induction and metabolism. *Biomaterials* 2023;292.
24. Wang W, Taufalele PV, Millet M, *et al*. Matrix stiffness regulates tumor cell intravasation through expression and ESRP1-mediated alternative splicing of MENA. *Cell Rep* 2023;42:112338.
25. Ferreira S, Saraiva N, Rijo P, *et al*. LOXL2 Inhibitors and Breast Cancer Progression. *Antioxidants (Basel)* 2021;10:312.
26. Peoples JN, Saraf A, Ghazal N, *et al*. Mitochondrial dysfunction and oxidative stress in heart disease. *Exp Mol Med* 2019;51:162:1–13:.
27. Wang Y, Huang T, Gu J, *et al*. Targeting the metabolism of tumor-infiltrating regulatory T cells. *Trends Immunol* 2023;44:598–612.
28. Rao D, Verburg F, Renner K, *et al*. Metabolic profiles of regulatory T cells in the tumour microenvironment. *Cancer Immunol Immunother* 2021;70:2417–27.
29. Liu B-H, Xu C-Z, Liu Y, *et al*. Mitochondrial quality control in human health and disease. *Mil Med Res* 2024;11:32.
30. Wang Z, Lu Z, Lin S, *et al*. Leucine-tRNA-synthase-2-expressing B cells contribute to colorectal cancer immunoevasion. *Immunity* 2022;55:1748.
31. Leask A, Nguyen J, Naik A, *et al*. The role of yes activated protein (YAP) in melanoma metastasis. *i Sci* 2024;27:109864.
32. Wang Z, Lu Z, Lin S, *et al*. Leucine-tRNA-synthase-2-expressing B cells contribute to colorectal cancer immunoevasion. *Immunity* 2022;55:1067–81.
33. Qu Y, Wang X, Bai S, *et al*. The effects of TNF-α/TNFR2 in regulatory T cells on the microenvironment and progression of gastric cancer. *Int J Cancer* 2022;150:1373–91.
34. Golo M, Newman PLH, Kempe D, *et al*. Mechanoimmunology in the solid tumor microenvironment. *Biochem Soc Trans* 2024;52:1489–502.
35. Shi L, Lim JY, Kam LC. Improving regulatory T cell production through mechanosensing. *J Biomed Mater Res A* 2024;112:1138–48.
36. Jairaman A, Othy S, Dynes JL, *et al*. Piezo1 channels restrain regulatory T cells but are dispensable for effector CD4$^+$ T cell responses. *Sci Adv* 2021;7:eabg5859.
37. Li H, Luo Q, Shan W, *et al*. Biomechanical cues as master regulators of hematopoietic stem cell fate. *Cell Mol Life Sci* 2021;78:5881–902.
38. Hu L, Ni F, Wang X, *et al*. Decreased cell stiffness enhances leukemia development and progression. *Leukemia* 2020;34:2493–7.
39. Suomalainen A, Nunnari J. Mitochondria at the crossroads of health and disease. *Cell* 2024;187:2601–27.
40. Wang Y, Ruan L, Zhu J, *et al*. Metabolic regulation of misfolded protein import into mitochondria. *Elife* 2024;12.
41. Su É, Villard C, Manneville J-B. Mitochondria: At the crossroads between mechanobiology and cell metabolism. *Biol Cell* 2023;115:e2300010.